SUBMISSION TO
CONSTRUCTION AND BUILDING MATERIALS

DATE:
Revised: May 2021

TITLE:
An experimental investigation into the use of mica as a material for the stabilisation of marginal clays in construction

AUTHORS:
Christopher U. Ibeh
Alessandro Tarantino
Matteo Pedrotti
Rebecca J. Lunn

AFFILIATION:
Department of Civil and Environmental Engineering, University of Strathclyde, Glasgow, UK

CORRESPONDING AUTHOR:
Mr Cristopher Ibeh
Department of Civil and Environmental Engineering
University of Strathclyde
James Weir Building - Level 5
75 Montrose Street - Glasgow G1 1XJ, Scotland, UK
E-mail : christopher.ibeh@strath.ac.uk

KEYWORDS
Muscovite, shear strength, hydraulic conductivity, marginal clay, kaolin, circular economy
Number of words: 53334
Number of figures: 17
Number of tables: 2

An experimental investigation into the use of mica as a material for the stabilisation of marginal clays in construction

Abstract

The scarcity and cost of high-quality construction materials have resulted in their use being reserved for the construction of structures that experience relatively high stress, such as roads with high traffic volumes. Consequently, mechanically improved abundant marginal materials are common in relatively low stress construction applications such as landscaping, low-volume paved roads and fill material for flood embankments. In clays, mechanical improvement is commonly achieved through the addition of chemical stabilizers such as lime, bitumen, cement, and fly ash. However, these chemical stabilizers are associated with high cost and a large carbon footprint. Here, we present the first research demonstrating that clays can be mechanically improved through the addition of mica. Mica wastes are generated in significant volume as a by-product from the mining of relatively valuable materials. This paper explores the use of mica to improve the ultimate limit state of marginal clays for use as construction material. Kaolin clay was prepared with muscovite sand and muscovite silt in variable fractions (0%, 2.5%, 10% and 30% muscovite fraction). The hydraulic and mechanical response of the composite materials were investigated through one-dimensional compression and direct shear testing. The most notable finding is that, at very low normal stresses (≤100 kPa), a relatively small fraction of mica is sufficient to shift the angle of shearing resistance of the composite, from the value for pure clay (ϕ'~17°) towards the value for pure muscovite (ϕ'~26°). X-ray computed tomography scans of the consolidated and sheared samples show that the relatively high strength of the mica clay composite at low normal stress is due to a fold-like mode of deformation observed in shearing. This mechanism appears to be suppressed at high stresses with the shear band likely developing through the clay matrix. As a result, the composite exhibits the same friction angle of the clay alone at high stresses.

Keywords: Mica, shear strength, hydraulic conductivity, marginal clay, kaolin, circular economy

1 Introduction

In recent years, the scarcity and cost of high-quality construction materials have resulted in their use being reserved for the construction of structures that will experience relatively high stress, such as roads with high traffic volumes [1]. Consequently, abundant marginal materials are common in relatively low stress geotechnical applications such as landscaping, low-volume paved roads and fill material for flood embankments. Further, the use of local marginal materials can result in significant carbon savings [1–6] as well as enhancing the drive towards a circular economy [1,7,8].

Marginal materials are defined as materials that do not possess, in their present form, quality levels that meet current standards sufficient for their use as various structural components. Thus, their properties need to be improved mechanically. Chemical stabilizers such as lime, bitumen, cement, and fly ash have successfully been used in the past to improve the performance of some marginal clays [1,9–11]. However, these chemical stabilizers are associated with high cost and a large carbon footprint [12]. By-product mica could prove a valuable alternative to improve the mechanical performance of marginal clays.

A significant amount of mining by-product is mica generated both from the mining of relatively valuable materials such as gold, copper, uranium and platinum [13] and that of less valuable materials such as china clay [14] and mica itself [15]. About 10 million tons of mica waste is generated in a year and over 600 million tons of total industry stockpile are estimated to be available [16]. Due to its abundance, researchers have begun to explore its use in construction. Mica has high radiation resistance and good insulation properties [17] and has been shown to have good thermal and mechanical properties. For example, [18,19] observed that the mechanical and thermal properties of glass-mica composites are superior to those of conventional building materials, such as concrete, masonry products and cement mortar.

Similarly, [20], demonstrated the possibility of using a tungsten mine waste, containing mica and quartz, to produce alkali activated binders using a calcination process. To-date, the proposed applications for mica in construction use processes that expend relatively large amounts of energy (calcination and glass manufacture). Whilst highly valuable, these high energy applications may not be desirable for the full 600 million ton backlog of mica waste now stockpiled. There is, therefore, scope to investigate lower-energy applications of waste mica in construction.

This paper explores the feasibility of using by-product mica for enhancing the mechanical properties of marginal clay for low stress applications in construction. The paper presents an evaluation of the shear strength, compressibility and hydraulic conductivity of muscovite and kaolin composites for geotechnical uses such as structural fills and landscaping. Speswhite kaolin clay was mixed with variable weight percentages of muscovite silt or sand, in the ratios 0%, 2.5%, 10% and 30% by weight of muscovite. The hydraulic and mechanical behaviour of these composite materials was then tested via one-dimensional compression and direct shear tests. Finally, sub-samples from the sheared specimens were imaged using X-ray computed tomography to enable an evaluation of the microscale mechanisms controlling the macroscopic behaviour of these composite materials.

2 Materials and specimen preparation

Three different materials were used in this study: Kaolin, Muscovite silt and Muscovite sand (Figure 1). Composite specimens made up of muscovite silt or sand mixed with kaolin in the ratios 2.5:97.5, 10:90, and 30:70 by weight were prepared and tested.

(a) (b) (c)

Figure 1. Images of (from left to right) kaolin, muscovite silt and muscovite sand used in this study

Speswhite kaolin with a liquid limit w_L= 0.64 and a plastic limit w_P=0.32 was used in the experiments. The grain size distribution, obtained through Laser diffraction analysis, is characterised by 80% clay-fraction (fraction < 2 micrometer) and 20% silt-fraction (fraction 2-63 micrometer). Muscovite silt used for this study was purchased from LKAB minerals Ltd. The muscovite silt has a median diameter d_{50} = 30 μm, particle sizes in the range 1 - 87 μm (obtained through Laser diffraction analysis) and a specific gravity of 2.8. Its chemical composition obtained with Micro- X-ray Fluorescent (Micro XRF) spectrometer performed at Bruker AXS is shown in Table 1. Muscovite sand was purchased from Specialist Aggregates Ltd. The muscovite sand has a median diameter, d_{50} = 1.5 mm, particle sizes in the range 0.25—2.8 mm, and a specific gravity of 2.8 (see figure 1c). Its chemical composition obtained through Micro XRF is shown in Table 1.

Table 1. Chemical composition of muscovite silt, muscovite sand and kaolin used in this study.

Element	Atomic Number	Compound	Normalized Stoichiometric Composition (wt.%)		
			Muscovite Silt	Muscovite Sand	Kaolin
Al	13	Al_2O_3	32	30 – 36	38
Si	14	SiO_2	43	43 – 50	47
K	19	K_2O	13	<9 -12	
Ti	22	TiO_2	1	1	

Fe	26	Fe_2O_3	8	1 – 5	-
Loss on ignition			Max 5%	Max 5%	

The kaolin and muscovite were supplied as dry powders/grains. We mixed the sample with a spatula until a homogeneous mixture was obtained, as determined by visual inspection since the colours of clay and mica particles are very different. To reconstitute kaolin clay and mica composite from slurry, distilled water was added to the dry powder up to a water content 1.5 times the liquid limit of kaolin (wL=0.64) following the procedure suggested by [21]. The reconstituted slurry preparation was used to better understand the intrinsic properties (devoid of field depositional conditions, ageing, cementation, and leaching) of the natural clay which is a robust frame of reference against which to assess the in-situ state of the clays. Slurry samples were used for both oedometer and direct shear tests. Samples were reconstituted from slurries prepared at the same initial water content to ensure that the different compression behaviour of the composites is only associated with its intrinsic properties (and not biased by differences in the initial conditions)

3 Experimental procedure

3.1 Direct Shear Tests

Drained direct shear box tests were conducted using a digital direct shear apparatus (ELE International, Sheffield, UK) according to the BS1377 standard [22], see figure 2 for typical setup for a direct shear test. The shear box has internal dimensions of 60 × 60 mm and accommodates specimens up to 20 mm height. The apparatus is equipped with a 5 kN capacity load cell and two displacement transducers to measure the shear force and both the vertical and shear (horizontal) displacements.

From the specimen consolidation data, it was determined that a shearing rate of 0.01 mm/min was sufficient to prevent pore water pressure build-up and thus maintain drained conditions during shearing. With the exception of the 100% kaolin sample, all specimens were sheared at this rate. For comparison with the composite materials, shear tests performed on the 100% kaolin clay, reconstituted from slurry and consolidated to 50, 100, and 150, are reported here taken from [23], with a shearing rate of 0.02 mm/min, and for the specimen consolidated to 300 kPa from [24], with shearing rate of 0.005 mm/min.

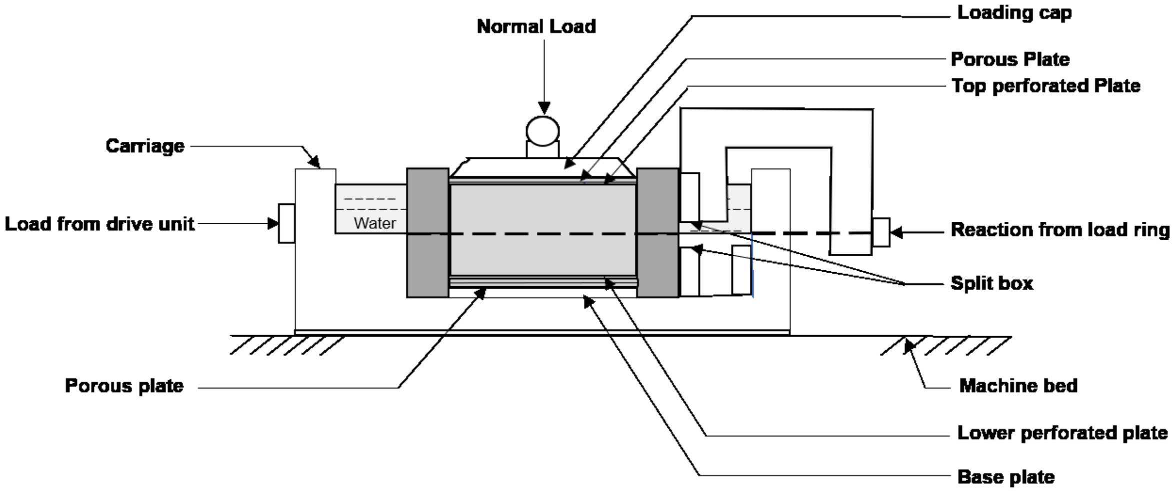

Figure 2: Typical setup for a direct shear test

3.2 One-dimensional (oedometer) compression tests

One dimensional oedometer compression tests were performed in a front-loading oedometer cell -diameter 75 mm (Controls Testing Equipment Ltd) according to [25], see figure 3 for a typical setup of an oedometer cell. Prior to loading, all samples were submerged under water in the oedometer cell. Samples were compressed in incremental steps starting from 3kPa vertical stress and doubling the load up to 2230kPa vertical stress. Unloading was performed in five steps.

For each loading and unloading step, samples were allowed to consolidate, i.e. the subsequent loading step was only applied when the secondary compression branch of the consolidation curve was clearly visible. The change in void ratio associated with a given loading step was computed by taking into account the change in the void ratio accumulated in the current loading step, due to primary consolidation, and the change in void ratio accumulated in the previous loading step, due to secondary consolidation (see Appendix I).

For each loading step, the consolidation time t_{50} associated with 50% consolidation was calculated and this enabled estimation of the consolidation coefficient c_v and, hence, the hydraulic conductivity *k* as detailed in Appendix II.

The void ratio associated with each imposed vertical stress was calculated backwards from the final specimen water content, the dry mass, and the specimen cross sectional area.

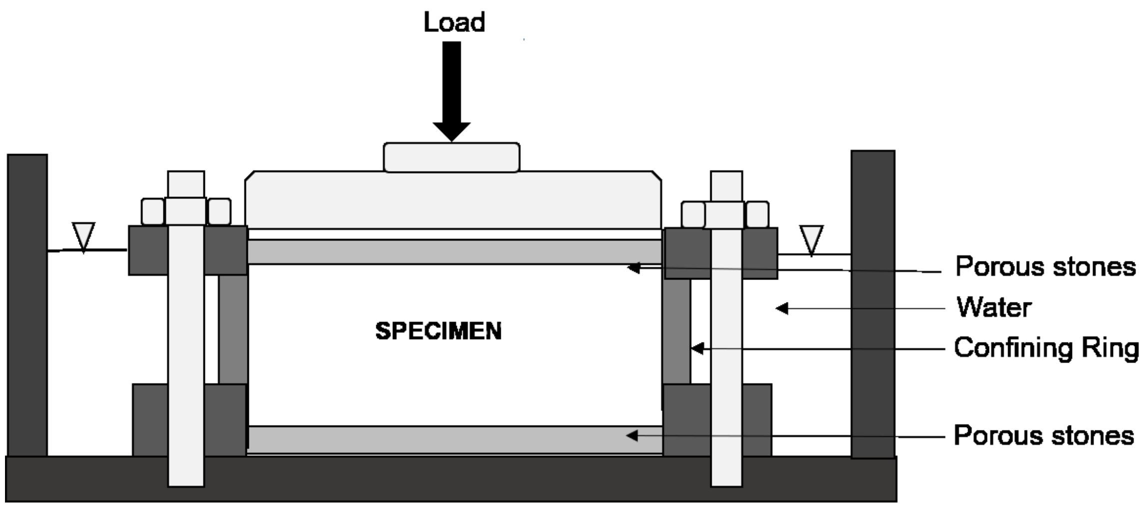

Figure 3: Typical setup of an oedometer cell

3.3 X-ray Computed Tomography

X-ray tomographies of the sample were performed with a Nikon XT H 320, see figure 4 for details of the X-ray computed tomography setup. The scan was performed using 3141 projections during a single revolution at 125kV energy and 108 μA current. The samples scanned were cylindrical samples cut out of consolidated or consolidated and sheared specimens with ~ 20 mm in diameter and the full sample height (after consolidation). The voxel size was 14.19 × 14.19 × 14.19 µm. The samples were covered with Parafilm® to maintain a constant water content during the scan and the tomographies were reconstructed using Nikon metrology X-Tek software and visualised using Thermo Fisher Scientific Avizo software.

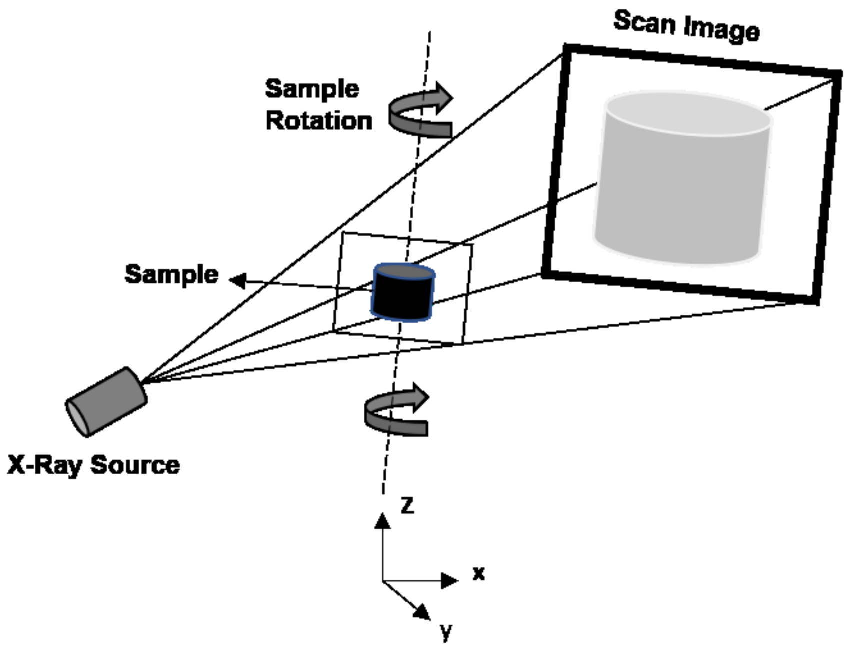

Figure 4: Typical X-ray computed tomography setup.

4 Results

4.1 Shear strength behaviour of kaolin-mica composites

Figure 5 (a, b, c, d, e) shows the results of direct shear tests performed on 100% kaolin, 10% muscovite sand/kaolin composite, 100% muscovite silt, 10% muscovite silt/kaolin composite and 100% muscovite sand, respectively. The kaolin, 10% muscovite sand/kaolin composite and muscovite silt and muscovite sand all exhibit a monotonic increase in shear stress up to the ultimate value and a contractile volumetric behaviour. This is the typical behaviour for the composite. It is worth noting that for both the kaolin and muscovite, the curves, in terms of the shear displacement versus the ratio between shear stress τ and normal effective stress σ', overlap. This indicates that the failure envelopes in the Mohr-Coulomb plane σ'- τ [26] for both the muscovite and the clay are linear and pass through the origin as shown in Figure 6. The experimental data for muscovite silt and muscovite sand lie almost perfectly along a linear failure envelope, with the exception of the data point associated with muscovite sand at 300 kPa vertical stress (see figure 6). The angle of shearing resistance for both the muscovite silt and the muscovite sand was found to be ϕ'=25.8° while the angle of shearing resistance for kaolin was found to be ϕ'=17.8°.

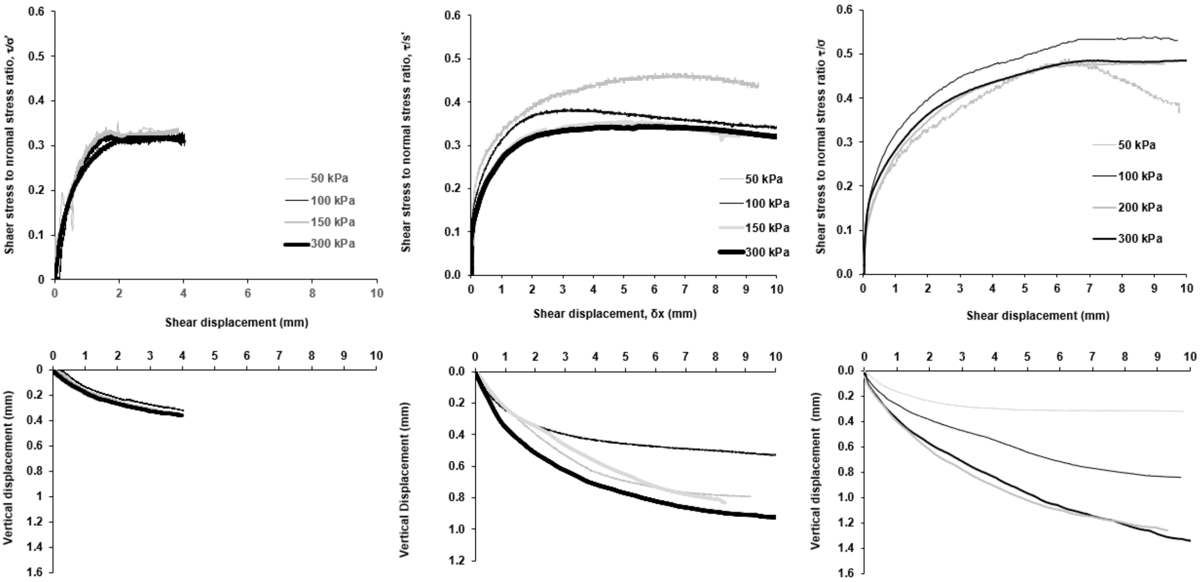

(a) (b) (c)

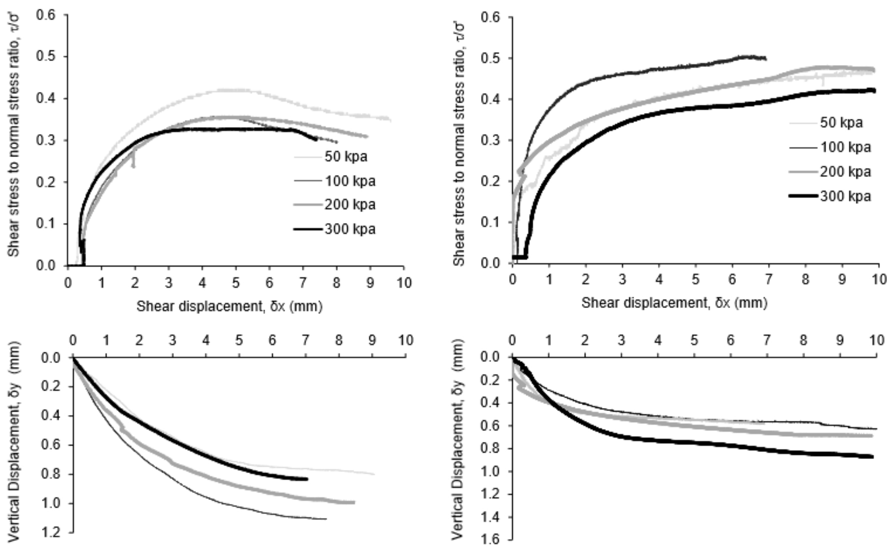

(d) (e)

Figure 5. Results of direct shear tests in terms of i) shear stress to normal stress ratio versus shear displacement and (plotted at the top of each figure) ii) vertical displacement versus shear displacement (plotted at the bottom of each figure). (a) 100% kaolin (b) 10% muscovite sand kaolin composite (c) 100% muscovite silt (d) 10% muscovite silt kaolin composite (e) 100% muscovite sand

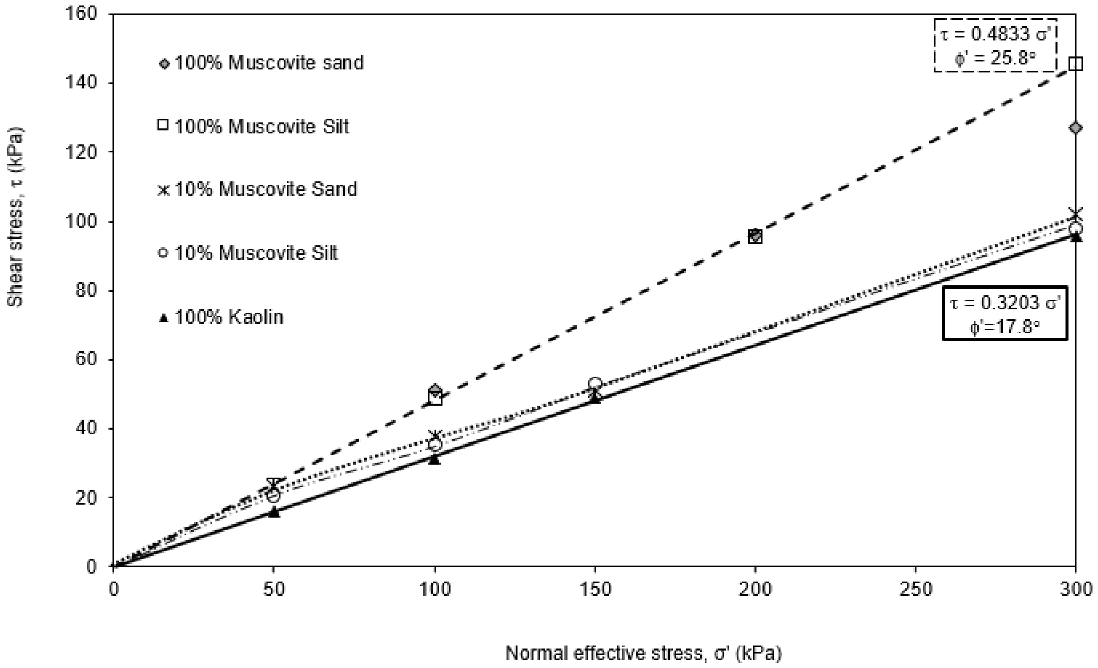

Figure 6. Failure envelope in terms of ultimate shear strength versus normal effective stress of muscovite silt, muscovite sand, kaolin and muscovite/kaolin composite.

To better appreciate the variations in shear strength with increasing normal effective stress, for the various muscovite/kaolin composites, Figure 7 shows the shear stress to normal effective stress ratio vs. the normal effective stress. As expected, the shear strength of the kaolin/ muscovite composites increases toward the value of the shear strength of the muscovite alone as the muscovite fraction increases. However, the most striking aspect of Figure 7 is that a relatively small fraction of muscovite (30%) is sufficient to shift the shear strength to the shear strength of the muscovite alone in the range of low effective normal stresses ($\sigma' \leq 50\text{-}100$ kPa). Further, even for smaller muscovite fractions (2.5% and 10%) there is still a significant increase in shear strength at low effective normal stresses. This effect vanishes as the normal effective stress increases (σ' = 200-300 kPa); at a normal effective stress of 300 kPa, the only sample that still shows some increase in shear strength is the 30% fraction of mica sand (Figure 7b).

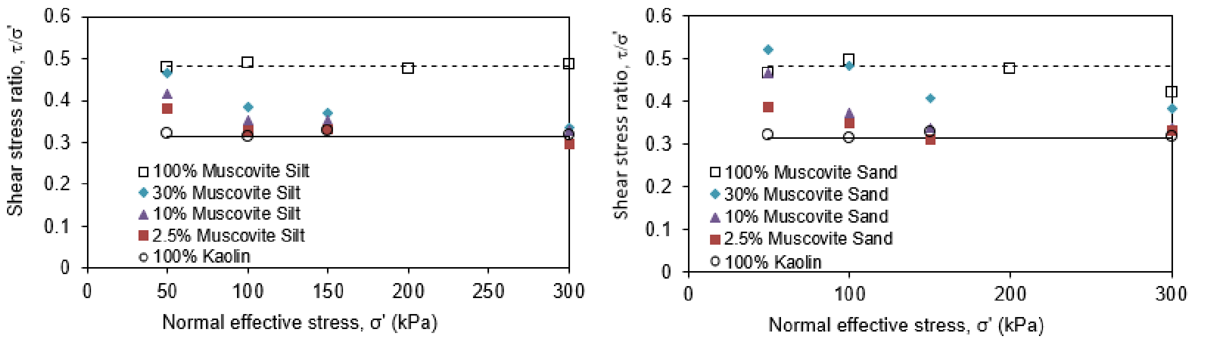

(a) (b)

Figure 7. Shear stress to normal effective stress ratio versus normal effective stress. (a) muscovite silt-kaolin composite. (b) muscovite sand-kaolin composite

4.2 1-D compression behaviour of kaolin-mica composites

Figure 8 shows the 1-D compression curves of the clay-muscovite-silt composites at varying proportions from 0% muscovite (100% kaolin) through 2.5%, 10, and 30% muscovite. The compression curves of the kaolin-muscovite silt composites essentially overlap with the compression curve of the kaolin alone, indicating that compression behaviour of the composites is dominated by the clay matrix regardless of the muscovite silt fraction (in the range 0-30%).

The compression curve for the muscovite silt alone presents an inflection at around 20 kPa vertical stress before becoming linear beyond 200 kPa vertical stress. The normal compression line of the muscovite silt is clearly located above the normal compression line of the kaolinite, which further corroborates the finding that the compression behaviour of the kaolin-muscovite silt composites are dominated by the clay matrix.

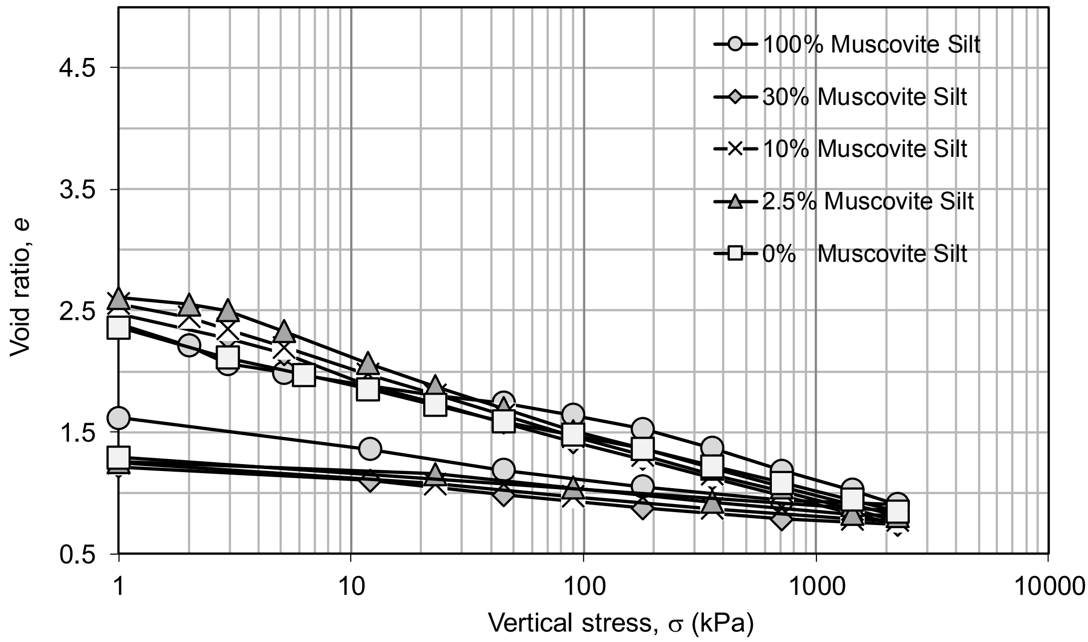

Figure 8. Oedometer compression curve of muscovite silt and kaolin composites

Figure 9 shows similar 1-D compression curves for the clay-muscovite-sand composites. Again, the compression curves of the kaolin-muscovite sand composites essentially overlap with the compression curve of the kaolin alone indicating that compression behaviour of the composites is dominated by the clay matrix.

The compression curve for the muscovite sand alone presents an abnormal initial void ratio. It is not clear whether this is due to an error in the computation of the void ratio change upon the first loading steps due to 'wall effects' at the interface between the top surface of the specimen and the loading cap (void ratio change would have been overestimated), or as a result of swelling occurring upon flooding of the oedometer cell (the water content of the initial slurry was the same for all the specimens tested). Unfortunately, the compression test of the muscovite sand alone could not be repeated. Table 2 shows the secant compression index of mica silt and mica sand composite obtained for vertical stress values between 100 and 2000 kPa.

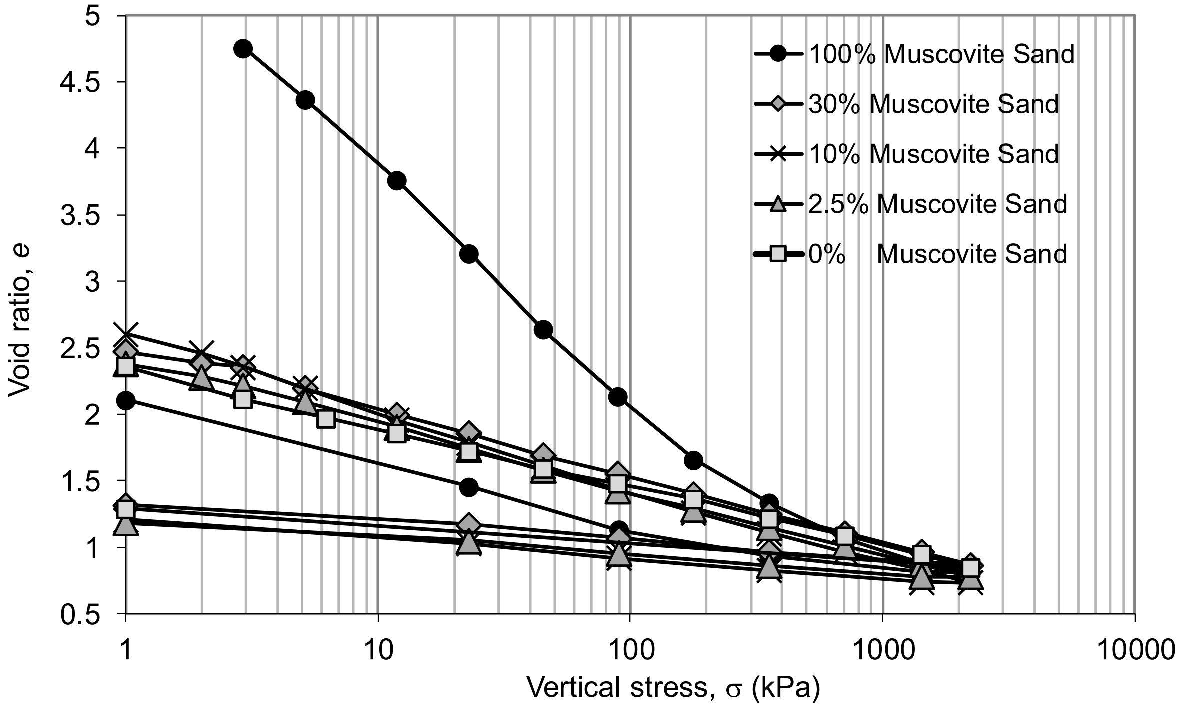

Figure 9. Oedometer compression curve of muscovite sand and kaolin mixture

Table 2: Compression index for mica sand and mica silt

	Mica Silt Compression index	Mica Sand Compression Index
0% (Kaolin)	0.19	0.19
2.50%	0.21	0.19
10%	0.21	0.21
30%	0.21	0.21
100%	0.22	0.40

There was no evidence of muscovite particle crushing in either the muscovite silt or sand; Figure 10 shows there was no change in the laser diffraction particle size analysis of the specimens before and after compression.

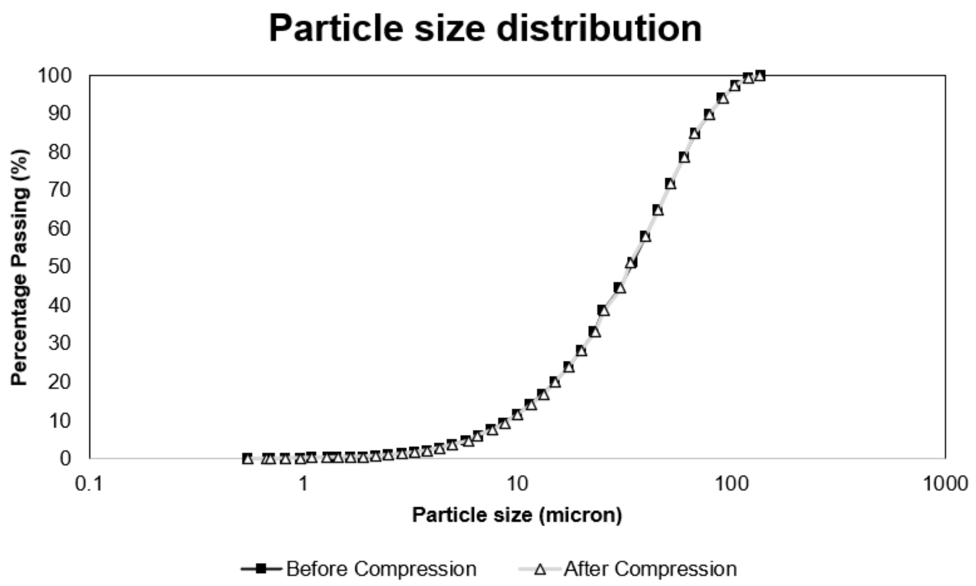

Figure 10: Mica particle size distribution before and after compression

4.3 Hydraulic conductivity of kaolin-muscovite composites

The hydraulic conductivity of the kaolin-muscovite composites was derived from the consolidation response upon individual loading steps based on Terzaghi's theory of one-dimensional consolidation [26] (Appendix II). As shown by [27], the values of hydraulic conductivity inferred from the consolidation data are consistent with the values measured experimentally via standard constant head/falling head hydraulic conductivity tests.

Hydraulic conductivity is plotted against vertical stress for both the muscovite silt composites and the muscovite sand composites in Figure 11. As expected, the hydraulic conductivity decreases as the vertical stress increases and, hence, the void ratio decreases (Figures 11a and 11b). The percentage of mica added (2.5% - 30%) does not significantly affect the hydraulic conductivity of the composite material compared to the clay. Therefore, up to 30% mica, the hydraulic conductivity remains controlled by the finer fraction.

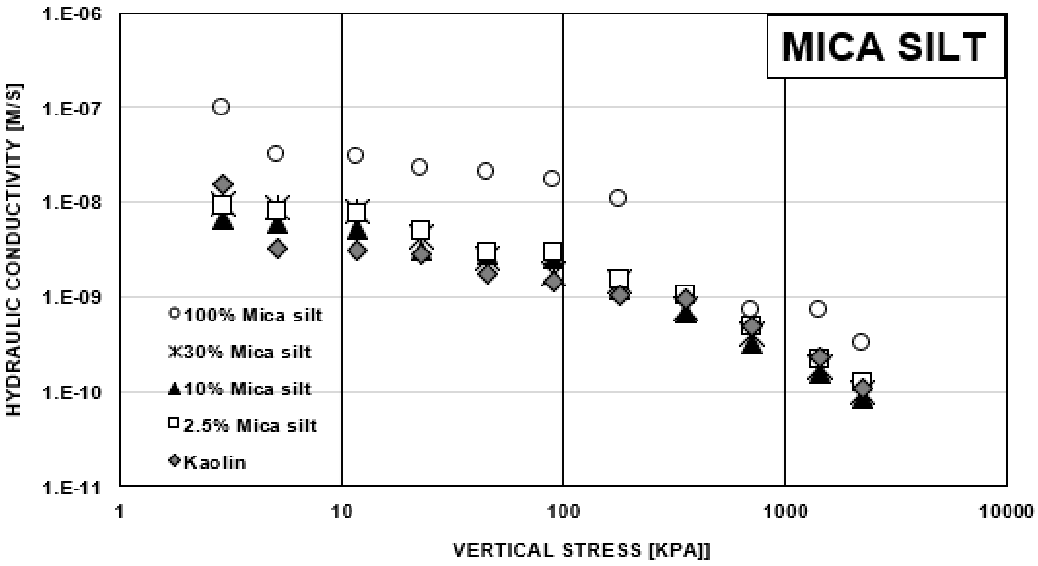

(a)

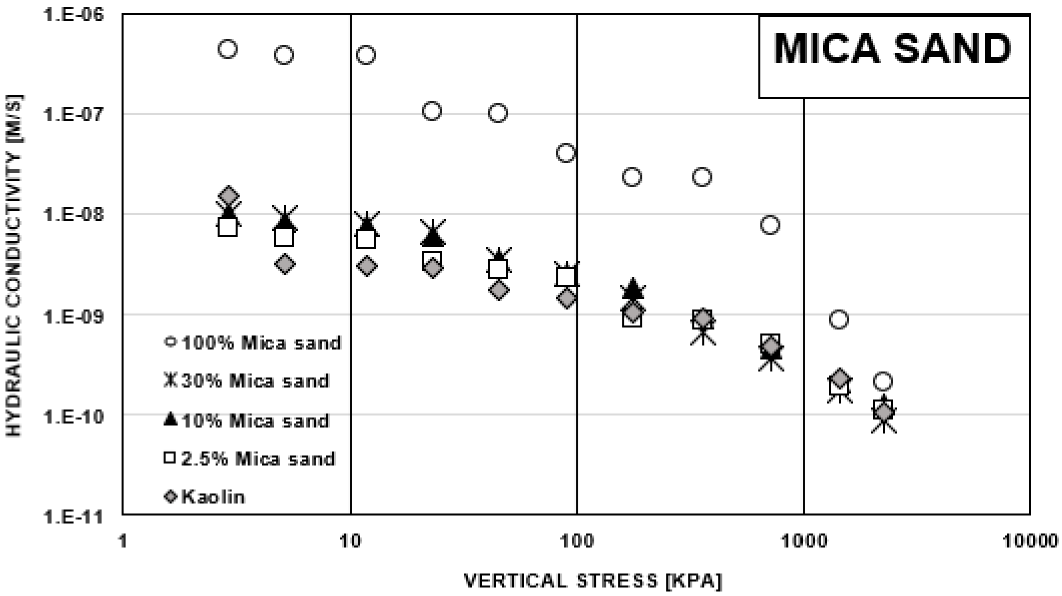

(b)

Figure 11. Hydraulic conductivity versus vertical stress. (a) kaolin-muscovite silt composites. (b) kaolin-muscovite sand composites.

4.4 X-ray CT slices of consolidated and sheared samples

Figures 12a, b show X-ray CT slices of two samples of the sand sized mica mixed with kaolin (30 percent mica sand) after consolidation to 50 kPa and 300 kPa vertical effective stress respectively. Mica sand particles appear to be randomly oriented in both samples, which is a reflection of the process of hand mixing of the composite material in its slurry state.

Figures 12c and d show the same specimens after shearing. The dashed line represents the position of the joint between the bottom and top halves of the shear box. Figure 12c (the sample sheared after compression to 50 kPa) shows preferential orientation of mica particles in the shearing zone whereas figure 12d (the sample sheared after consolidation to 300 kPa) shows that mica particles remained randomly oriented in the shearing zone.

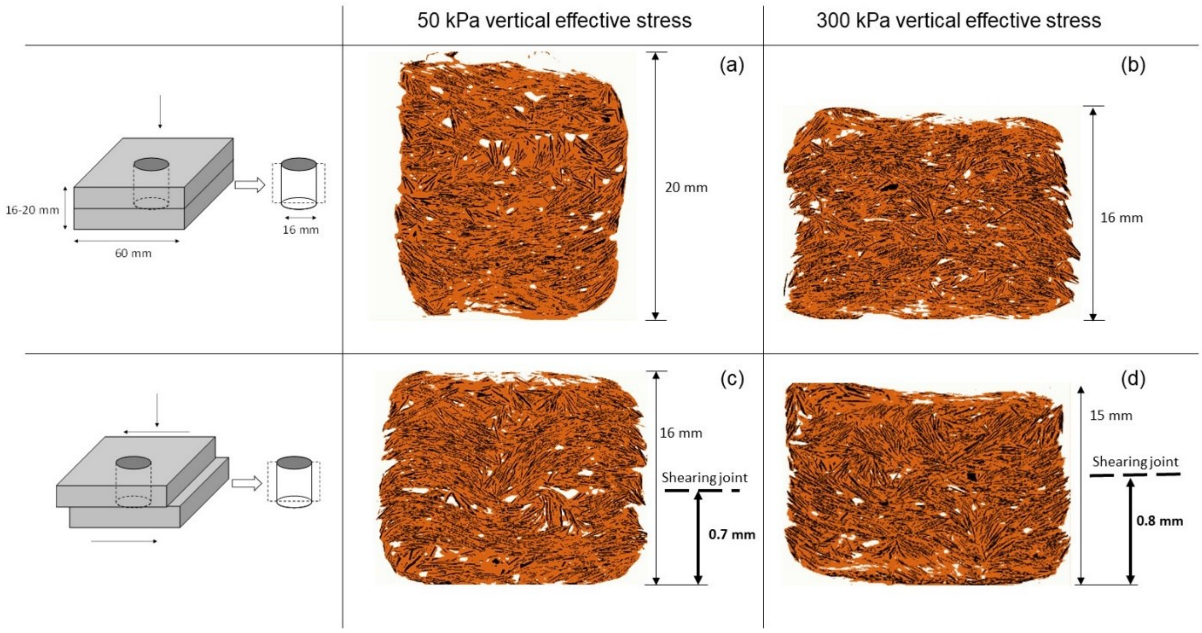

Figure 12: X-ray CT slices of (a) mica sand and kaolin consolidated to 50 kPa (b) mica sand and kaolin consolidated to 300 kPa (c) mica sand and kaolin consolidated to 50 kPa and shared (d) mica sand and kaolin consolidated to 300 kPa and sheared.

5 Discussion

The results from the oedometer tests, in terms of compressibility and hydraulic conductivity of the muscovite/kaolin composites show that behaviour in compression remains dominated by the clay matrix. It was not unexpected that a muscovite fraction up to 30% is not large enough to modify the compressional behaviour, which remains dominated by the clay matrix.

Similarly, for the hydraulic conductivity behaviour, mica particles 'float' within the clay matrix and this results in no significant hydraulic conductivity change of the composites (for up to 30% mica) compared to the value for mica alone.

By contrast, the shear strength data are not intuitive and, at the same time, have significant practical relevance. The range of low normal effective stresses where a relatively small fraction of muscovite generates a significant increase in shear strength ($\sigma' \leq 50$-100 kPa) are representative of the range of stresses developing in earth structures such as flood and roadway embankments and in the backfill of retaining structures. As a result, the addition of only 10-30% of muscovite silt or sand to the clay, with the aim of improving the mechanical behaviour of marginal clays, can significantly enhance the mechanical response of such geostructures.

At a more fundamental level, it is surprising that a relatively small fraction of muscovite can shift the shear strength of kaolin-muscovite mixtures to values close to the ones of the muscovite alone at low normal effective stress. As the compression behaviour of the composite is dominated by the clay matrix, regardless of the muscovite fraction (in the range 0-30%), one would have expected the shear strength to be also dominated by the clay matrix. This is the case at relatively high normal effective stresses ($\sigma' > 100$ kPa) but not at low stresses ($\sigma' \leq 50$-100 kPa).

The kaolinite and the silt/sand mica alone exhibit ultimate shear strength that does not depend on the normal effective stress σ' (Fig. 7a and b). At ultimate (critical) state, it can be assumed that particles in the shearing zone are subjected to 'turbulent' mixing [28] and that the 'macroscopic' angle of shearing resistance depends on the degree of interlocking that is resisting to the sliding and rolling over of particles.

For the case of mica sand and silt, the interlocking would be higher due to the angularity of mica particles and the nature of inter-particle contact. As shown by the X-CT scan in figure 13, mica particles have a rough surface. This increases the degree of interlocking at the critical state and, hence, increases the ‘macroscopic’ angle of shearing resistance. This is consistent with the findings of [29] who have shown that particle angularity plays a key role in determining the critical state angle of shearing resistance. Experimental data have shown that the angle of shearing resistance of uniform sand can span over a very wide range depending on particle angularity, from 40° in the case of very angular sand particles to 20° for perfectly rounded particles (glass beads) [30]. At the same time, the frictional resistance at the inter-particle contact is relatively high being controlled by mechanical interactions (Figure 14a).

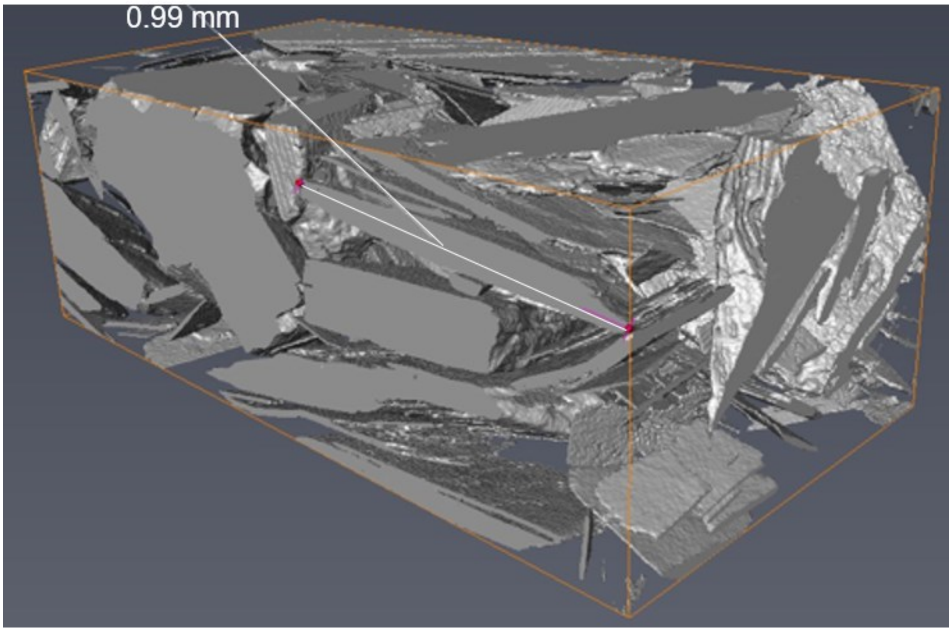

Figure 13 – X-CT image of mica sand

For the case of kaolinite, it may be that the particles are less angular and, most importantly, the normal stress at the inter-particle contact is diminished by the Coulombian repulsion occurring between the negatively charged particles. This would decrease the inter-particle frictional resistance facilitating particle sliding and rolling eventually leading to a lower macroscopic angle of shearing resistance (Figure 14b).

For the composite material, it is instructive to observe the orientation of the sand mica particles in the shearing zone. At low stress, mica particles highlight a pattern that resembles ductile shearing in geologically stratified layers, which are first folded and then broken by tectonic forces (Fig. 15a, c). The mica particles contribute to form ‘reinforced’ layers and the shearing process involves a fold-like mechanism rather than a particle-to-particle rolling and sliding. This could explain why the measured friction angle in mica sand composite at low stresses was observed to be even higher than mica sand alone (Fig. 7b).

At high vertical stress, the mica particles appear to preserve the same random orientation observed after compression (Fig. 15b). It can be speculated that the high vertical stress promotes the development of force chains mainly in the clay matrix and, hence, composite layers do not form upon macroscopic shearing. In this case, the shear band likely forms in the clay matrix (Fig. 15d) and this explains why the measured friction angle at high stresses in the mica sand composite is observed to be close to the value measured in the kaolinite alone (Fig. 7b).

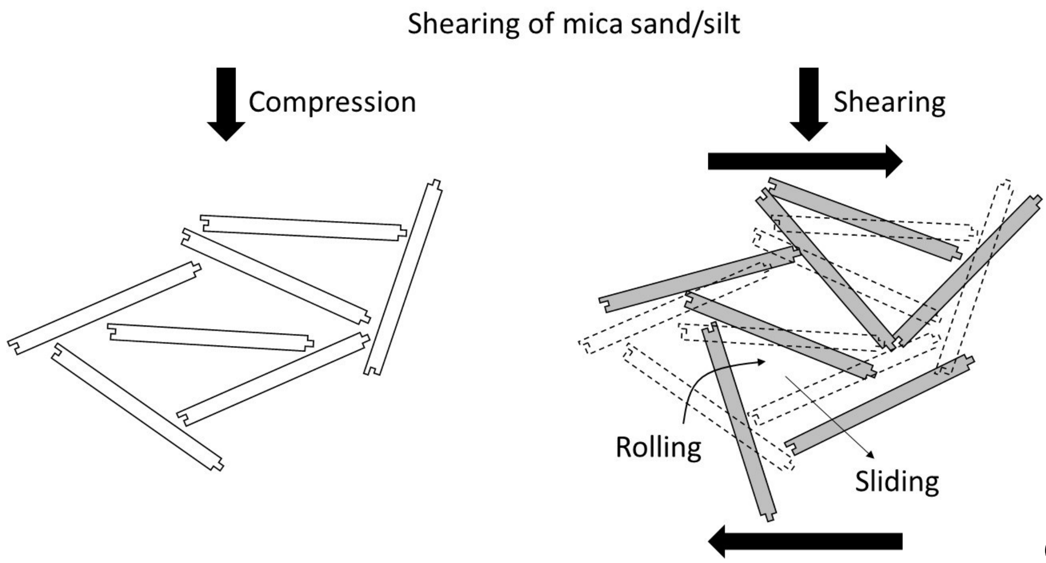

(a)

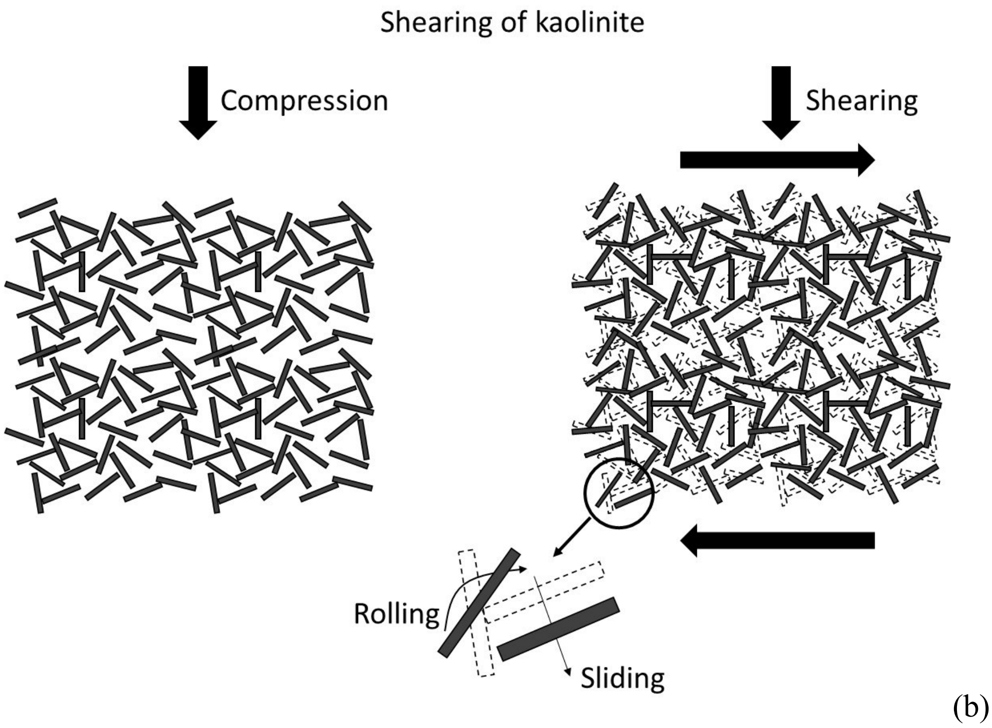

Figure 14. Conceptual model for response in shear of (a) mica sand/silt; (b) kaolinite

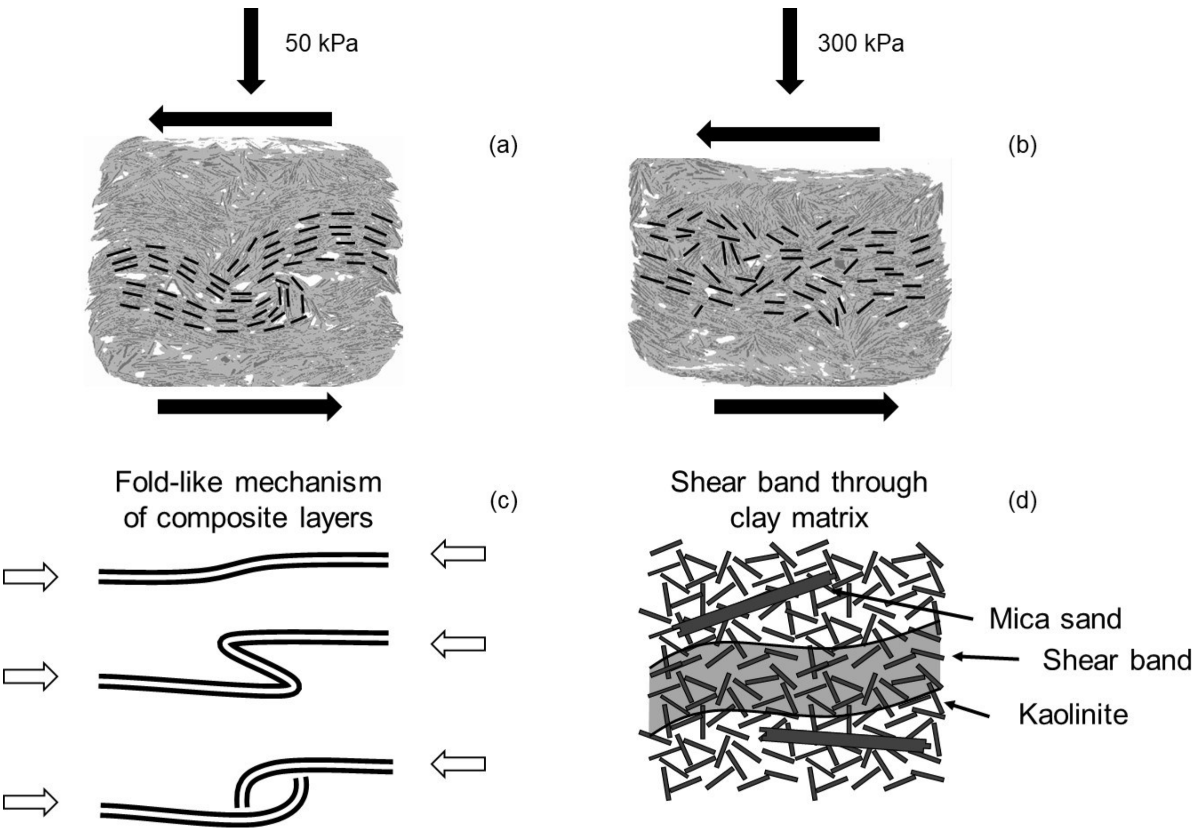

Figure 15. Response in shear of mica sand/silt and kaolinite composites. (a) preferential orientation of mica sand particles in the shearing zone at 50 kPa vertical stress. (b) random orientation of mica sand particles in the shearing zone at 300 kPa vertical stress. (c) Conceptual model for response in shear at low vertical stress. (d) Conceptual model for response in shear at high vertical stress

6 Conclusions

This paper has evaluated the compressibility, hydraulic conductivity, and shear strength characteristics of muscovite and kaolin composites for their use in low stress geotechnical regimes such as structural fills. Muscovite-kaolin composites were prepared with muscovite contents of 0, 2.5, 10, and 30 wt. %. It was observed that:

i) by adding both muscovite silt or muscovite sand to kaolin for all the weight percent of muscovite kaolin mixtures tested, compressibility does not change. Up to 30% muscovite sand or muscovite silt, the compressive behaviour is still clay-dominated.

ii) The addition of muscovite mica (up to 30%) to kaolin does not significantly affect its hydraulic conductivity. Hence a gain in shear strength does not compromise the hydraulic conductivity or compressibility of clay.

iii) The shear strength characteristics of kaolin are significantly enhanced by the addition of only 2.5-30% of muscovite silt or sand in the low stress regime typical of earth structures such as flood and roadway embankments and retaining structure backfill. Hence, whilst adding up to 30% mica to clay makes no significant difference to the hydraulic conductivity, it does improve the shear strength at low normal stresses.

These findings show that by-product mica significantly enhances the mechanical properties of marginal clays in low-stress, large-volume building applications such as structural fill. Considering the high cost and carbon footprint [12] of current systems, such as lime, bitumen, cement and fly ash [1,9–11], the addition of by-product mica as an alternative material for mechanical property enhancement in clays could reduce both the cost and environmental impacts of such applications. Mica-enhanced clay fills could also provide a low-cost, low-energy solution for the bulk of mica-based mine wastes, removing the current requirement for their active management and reducing their impact on the surrounding environment.

References

[1] J.J.E. Liebenberg, A.T. Visser, Stabilization and Structural Design of Marginal Materials for Use in Low-Volume Roads, Transp. Res. Rec. II (2003) 166–172. https://doi.org/10.3141/1819b-21.

[2] M. Ameri, A. Behnood, Laboratory studies to investigate the properties of CIR mixes containing steel slag as a substitute for virgin aggregates, Constr. Build. Mater. 26 (2012) 475–480. https://doi.org/10.1016/j.conbuildmat.2011.06.047.

[3] S.G. Choi, I. Chang, M. Lee, J.H. Lee, J.T. Han, T.H. Kwon, Review on geotechnical engineering properties of sands treated by microbially induced calcium carbonate precipitation (MICP) and biopolymers, Constr. Build. Mater. 246 (2020) 118415. https://doi.org/10.1016/j.conbuildmat.2020.118415.

[4] J.R. Cook, C.S. Gourley, A Framework for the Appropriate Use of Marginal Materials J R Cook C S Gourley, UK, TRL Ltd. 1 (2002) 1–19.

[5] K. Kalinowska-Wichrowska, E. Pawluczuk, M. Bołtryk, Waste-free technology for recycling concrete rubble, Constr. Build. Mater. 234 (2020) 117407. https://doi.org/10.1016/j.conbuildmat.2019.117407.

[6] F. Moreno, M.C. Rubio, M.J. Martinez-Echevarria, The mechanical performance of dry-process crumb rubber modified hot bituminous mixes: The influence of digestion time and crumb rubber percentage, Constr. Build. Mater. 26 (2012) 466–474. https://doi.org/10.1016/j.conbuildmat.2011.06.046.

[7] C.J. Kibert, Policy Instruments for Sustainable Built Environment, J. L. Use Environ. Law. 17 (2001). https://heinonline.org/HOL/Page?handle=hein.journals/jluenvl17&id=385&div=&collection=.

[8] A. Soleimanbeigi, T.B. Edil, Compressibility of Recycled Materials for Use As Highway Embankment Fill, J. Geotech. Geoenvironmental Eng. 141 (2015) 04015011. https://doi.org/10.1061/(asce)gt.1943-5606.0001285.

[9] G.N. Obuzor, J.M. Kinuthia, R.B. Robinson, Utilisation of lime activated GGBS to reduce the deleterious effect of flooding on stabilised road structural materials: A laboratory simulation, Eng. Geol. 122 (2011) 334–338. https://doi.org/10.1016/j.enggeo.2011.06.010.

[10] I. Phummiphan, S. Horpibulsuk, P. Sukmak, A. Chinkulkijniwat, A. Arulrajah, S.L. Shen, Stabilisation of marginal lateritic soil using high calcium fly ash-based geopolymer, Road Mater. Pavement Des. 17 (2016) 877–891. https://doi.org/10.1080/14680629.2015.1132632.

[11] E. Coudert, M. Paris, D. Deneele, G. Russo, A. Tarantino, Use of alkali activated high-calcium fly ash binder for kaolin clay soil stabilisation: Physicochemical evolution, Constr. Build. Mater. 201 (2019) 539–552. https://doi.org/10.1016/j.conbuildmat.2018.12.188.

[12] P. Sargent, P.N. Hughes, M. Rouainia, A new low carbon cementitious binder for stabilising weak ground conditions through deep soil mixing, Soils Found. 56 (2016) 1021–1034. https://doi.org/10.1016/j.sandf.2016.11.007.

[13] A. Nosrati, J. Addai-Mensah, W. Skinner, pH-mediated interfacial chemistry and particle interactions in aqueous muscovite dispersions, Chem. Eng. J. 152 (2009) 406–414. https://doi.org/10.1016/j.cej.2009.05.001.

[14] A. Zografou, A. Heath, P. Walker, China clay waste as aggregate in alkali-activated cement mortars, Proc. Inst. Civ. Eng. - Constr. Mater. 167 (2014) 312–322. https://doi.org/10.1680/coma.13.00037.

[15] B.B. Basak, Waste Mica as Alternative Source of Plant-Available Potassium: Evaluation of Agronomic Potential Through Chemical and Biological Methods, Nat. Resour. Res. 28 (2019) 953–965. https://doi.org/10.1007/s11053-018-9430-3.

[16] B. Palumbo-Roe, T. Colman, D.G. Cameron, K. Linley, A.G. Gunn, The nature of waste associated with closed mines in England and Wales, (2014) 82. http://nora.nerc.ac.uk/id/eprint/10083/.

[17] T. Shishelova, V. Zhitov, Radiation-resistant materials based on mica in the construction industry, MATEC Web Conf. 212 (2018) 1–6. https://doi.org/10.1051/matecconf/201821201012.

[18] N.L.P. Low, Formation and properties of glass-mica composite materials, Ceramurg. Int. 6 (1980) 85–90. https://doi.org/10.1016/0390-5519(80)90018-6.

[19] A. Mallik, Physico-mechanical behaviour of alkali and alkaline earth metal-containing mica glass–ceramics: a comparative evaluation, J. Korean Ceram. Soc. 57 (2020) 520–529. https://doi.org/10.1007/s43207-020-00054-9.

[20] F. Pacheco-Torgal, J. Castro-Gomes, S. Jalali, Tungsten mine waste geopolymeric binder: Preliminary hydration products investigations, Constr. Build. Mater. 23 (2009) 200–209. https://doi.org/10.1016/j.conbuildmat.2008.01.003.

[21] J.B. Burland, On the compressibility and shear strength of natural clays, Geotechnique. 40 (1990) 329–378. https://doi.org/10.1680/geot.1990.40.3.329.

[22] 1377-7 BS-CODE, Methods of test for soils for civil engineering purposes. Shear strength tests (total stress), 3 (1990).

[23] C. Wong, M. Pedrotti, G. El Mountassir, R.J. Lunn, A study on the mechanical interaction between soil and colloidal silica gel for ground improvement, Eng. Geol. 243 (2018) 84–100. https://doi.org/10.1016/j.enggeo.2018.06.011.

[24] A. Galvani, Resistenza a taglio di un argilla non satura ricostituita in laboratorio,

M.Eng., Univ. Trento. (2003).

[25] 1377-5 BS-CODE, Methods of test for soils for civil engineering purposes. Compressibility, permeability and durability tests, 3 (1990).

[26] Knappett. J & Craig R. F., Craig's Soil Mechanics, 8th ed, CRC press, 2012.

[27] M. Martini, A. Tarantino, A. Sloan, Suction drain as a low carbon ground improvement technique: Proof-of-concept at the laboratory scale, Tunn. Undergr. Sp. Technol. 99 (2020) 103361. https://doi.org/10.1016/j.tust.2020.103361.

[28] D.M. Wood, Soil behaviour and critical state soil mechanics, Cambridge University Press, 2014. https://doi.org/10.1017/CBO9781139878272.

[29] G.-C. Cho, J. Dodds, J.C. Santamarina, Particle Shape Effects on Packing Density, Stiffness, and Strength: Natural and Crushed Sands, J. Geotech. Geoenvironmental Eng. 132 (2006) 591–602. https://doi.org/10.1061/(asce)1090-0241(2006)132:5(591).

[30] K.A. Alshibli, M.B. Cil, Influence of Particle Morphology on the Friction and Dilatancy of Sand, J. Geotech. Geoenvironmental Eng. 144 (2018) 04017118. https://doi.org/10.1061/(asce)gt.1943-5606.0001841.

APPENDX I – Determination of void ratio change in oedometer compression.

Upon each loading and unloading step, specimens are allowed to complete primary consolidation. The completion of primary consolidation can be detected only when the secondary consolidation branch of the settlement versus time curve becomes clearly visible. As a result, the change in void ratio accumulated upon a loading or unloading step includes these two components. As shown in Figure 16, the primary consolidation is associated with an increase in effective stress whereas the secondary consolidation occurs at constant effective stress. The secondary consolidation at constant effective stress represents a change in void ratio that should have occurred in the subsequent loading step and should therefore be attributed to the subsequent loading step as shown in Fig. 16.

In other words, the change in void ratio Δe_i upon the i-th step associated with an increase in the effective stress $\Delta\sigma_i$, is given by

$$\Delta e_i = \Delta e_{i,primary} + \Delta e_{i-1,secondary} \qquad [1]$$

where $\Delta e_{i,primary}$ is the void ratio change associated with the primary consolidation of the step i and $\Delta e_{i-1,secondary}$ is the void ratio change associated with the secondary consolidation of the previous step *i-1*.

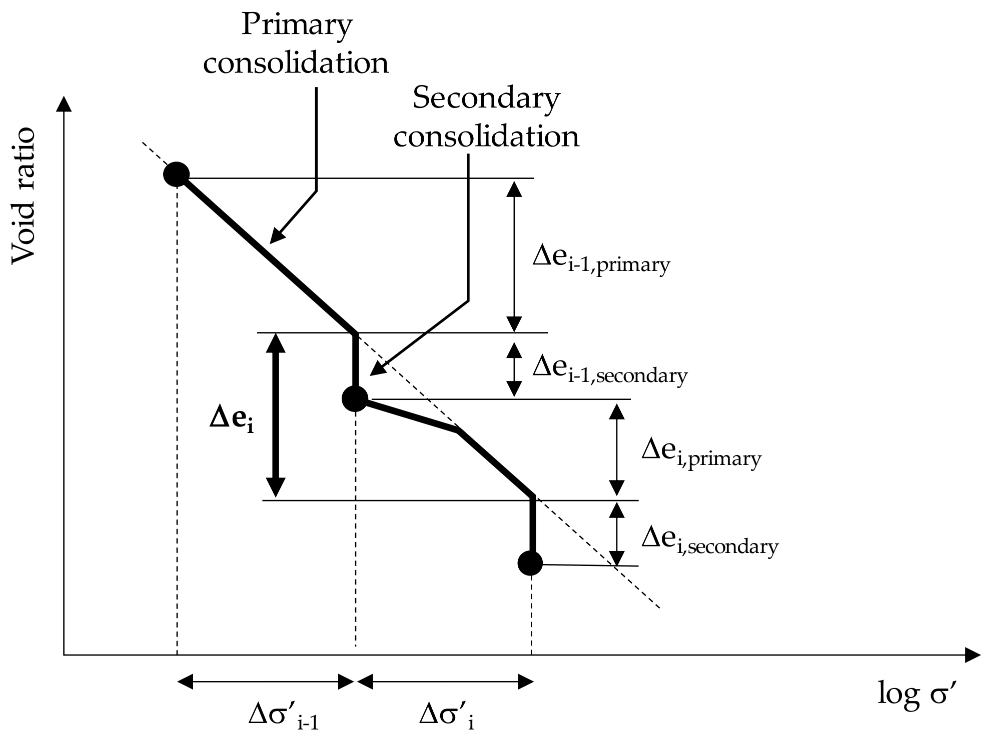

Figure 16. Computation of void ratio change Δe upon associated with an increment in effective stress $\Delta\sigma'$.

APPENDIX II – Determination of hydraulic conductivity from oedometer consolidation test

The hydraulic conductivity was determined as follows: The consolidation curve of each loading step was plotted, and the primary and secondary consolidation settlements were identified as shown in Fig. 17. The time t_{50} corresponding to 50% primary consolidation was then identified as shown in Figure 17 and the consolidation coefficient C_v computes as follows:

$$C_v = \frac{0.197\ h^2}{t_{50}} \qquad [2]$$

where 0.197 is the theoretical time factor corresponding to 50% consolidation and h is the drainage length (a standard oedometer consolidating test has double drainage and, as such, the specimen height is equal to $2h$).

The 1-D secant modulus E_{1D} was the calculated as

$$E_{1D} = \frac{\Delta б_i}{\varepsilon_i} \qquad [3]$$

where ε_i is the strain accumulated in the i-th loading step in turn given by:

$$\varepsilon_i = \frac{\Delta e_i}{1 + e_{0,\mathrm{i}}} \qquad [4]$$

where Δe_i and e_{0i} are the change in void ratio and the initial void ratio respectively in the i-th step. Finally, the hydraulic conductivity k was calculated as follows

$$k = \frac{C_v ɣ_w}{E_{1D}} \qquad [5]$$

where $ɣ_w$ is the unit weight of water.

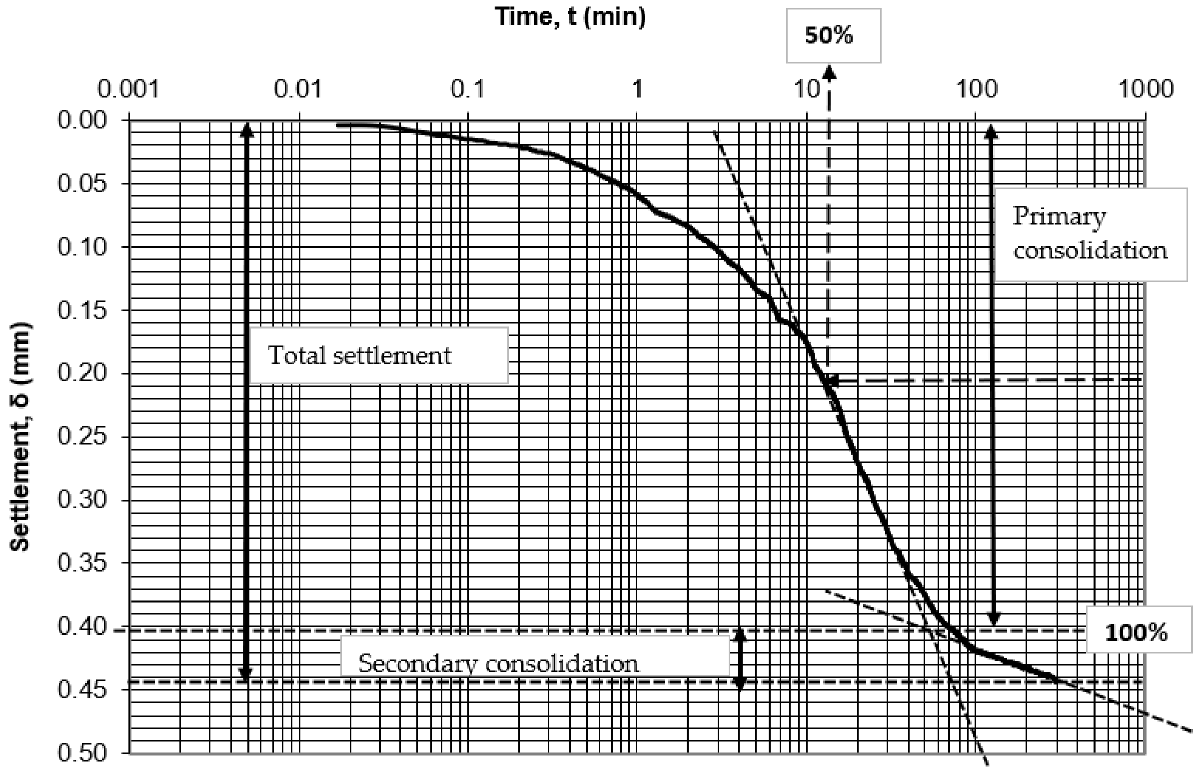

Figure 17. A typical consolidation curve for 2.5% muscovite and 97.5% kaolin at 3kPa loading step showing consolidation phases and analysis of log-time/settlement.